International Journal of Geo-Information

MDPI

*Article*

# Extraction of Urban Built-Up Areas Based on Data Fusion: A Case Study of Zhengzhou, China

**Yaping Chen [1] and Jun Zhang [2,*]**

[1] School of CML Engineering Architecture, Zhejiang Guangsha Vocational and Technical University of Construction, Jinhua 322100, China
[2] School of Architecture and Planning, Yunnan University, Kunming 650500, China
* Correspondence: 12017002153@mail.ynu.edu.cn

**Abstract:** Urban built-up areas are not only the spatial carriers of urban activities but also the direct embodiment of urban expansion. Therefore, it is of great practical significance to accurately extract urban built-up areas to judge the process of urbanization. Previous studies that only used single-source nighttime light (NTL) data to extract urban built-up areas can no longer meet the needs of rapid urbanization development. Therefore, in this study, spatial location big data were first fused with NTL data, which effectively improved the accuracy of urban built-up area extraction. Then, a wavelet transform was used to fuse the data, and multiresolution segmentation was used to extract the urban built-up areas of Zhengzhou. The study results showed that the precision and kappa coefficient of urban built-up area extraction by single-source NTL data were 85.95% and 0.7089, respectively, while the precision and kappa coefficient of urban built-up area extraction by the fused data are 96.15% and 0.8454, respectively. Therefore, after data fusion of the NTL data and spatial location big data, the fused data compensated for the deficiency of single-source NTL data in extracting urban built-up areas and significantly improved the extraction accuracy. The data fusion method proposed in this study could extract urban built-up areas more conveniently and accurately, which has important practical value for urbanization monitoring and subsequent urban planning and construction.

**Keywords:** urbanization; urban expansion; social remote sensing; urban built-up area; Zhengzhou



**Citation:** Chen, Y.; Zhang, J. Extraction of Urban Built-Up Areas Based on Data Fusion: A Case Study of Zhengzhou, China. *ISPRS Int. J. Geo-Inf.* **2022**, *11*, 521. https://doi.org/10.3390/ijgi11100521

Academic Editors: Hangbin Wu, Tessio Novack and Wolfgang Kainz

Received: 2 August 2022
Accepted: 14 October 2022
Published: 17 October 2022



## 1. Introduction

Urban built-up areas refer to areas that have undergone tract development and are equipped with basic municipal public facilities [1]. Urban built-up areas are the main areas in which human and economic activity are concentrated, and they are also the spatial carriers for urban activity [2]. Essentially speaking, urbanization is the transformation from rural areas to urban areas, along which the permanent manifestation is the extensive expansion of urban built-up areas. In other words, there is a close connection between the transformation of urban built-up areas and the urbanization level, which means that the accurate extraction of urban built-up areas would undoubtedly contribute to the knowledge of urbanization [3,4].

With the acceleration of China's urbanization in recent years, the urban built-up area in China has drastically increased. By 2020, the total urban built-up area of China has increased by 746% to 30,521.13 square kilometers since 1972 [5]. However, the main statistical data and extraction methods still rely on single-source and prolonged statistics and surveys, which can no longer meet the high-quality development requirements of China's new urbanization. The reality that urban built-up areas are experiencing drastic change calls for more accurate and more propagable methods for urban built-up area extraction [6,7]. However, at present, most of the studies on urban built-up areas focus on large cities with a higher development level and areas with larger built-up areas, while little attention is paid to cities that are still in the period of rapid development and with a general urban development level.

Thanks to the rapid development of remote-sensing technology, a series of remote-sensing data have gradually been used in urban-related studies, including nighttime light data (NTL) [8]. Nighttime light can represent the distribution of the population and infrastructure within urban cities by capturing urban nighttime light brightness, which is also the reason why NTL data are widely used in the analysis of human activity and the estimation of related social and economic factors [9–11]. Currently, the commonly used NTL data include DMSP/OLS (Defence Meteorological Program Operational Line-Scan System), NPP/VIIRS (Suomi National Polar-orbiting Partnership/Visible Infrared Imaging Radiometer Suite) and Luojia-01 data, among which the time scale of DMSP/OLS NTL data is from 1992 to 2013, the time scale of NPP/VIIRS NTL data is from 2012 and the time scale of Luojia-01 NTL data is from June 2018 to 2022. Although the latest Luojia-01 NTL data cannot be accessed since 2022, the original data can still be accessed. Second, compared with the DMSP/OLS data, the spatial resolution of the NPP/VIIRS data has increased by 500 m to 1000 m, which allows for finer details in urban-related studies [12–15]. In October 2018, Wuhan University launched the Luojia-01 experimental satellite, which began to provide high-resolution nighttime light data with a spatial resolution of 130 m. Compared with the DMSP/OLS and NPP/VIIRS data, the great improvement in the spatial resolution of the Luojia-01 data makes it possible to evaluate urban internal spatial structures in a fine way [16]. Additionally, the higher spatial resolution makes the urban internal spatial structure reflected by the Luojia-01 more complete. Therefore, the current application of the Luojia-01 data mainly focuses on the identification of urban spatial structures, the extraction of urban built-up areas and the delineation of urban boundaries. The Luojia-01 data have changed the study emphasis of NTL data from focusing on urban agglomerations and metropolitan areas to focusing on a single city [17,18].

Studies on the extraction of urban built-up areas based on NTL data started with the dichotomy method and threshold method, that is, on the premise that the built-up area and range of the target area are known, the values of NTL data are extracted so that the high-value range of the extracted nighttime light value is as close as possible to the known built-up area and range [19,20]. However, this method is too cumbersome to operate and requires a certain understanding of the study area, which makes it difficult to popularize the methods to a large area [21]. Therefore, the current studies on the extraction of built-up areas are mostly based on image segmentation, that is, the segmentation of NTL data, such as edge detection segmentation, feature segmentation, object-oriented segmentation, etc. [22–24]. Although these segmentation methods have achieved good results in the extraction of urban built-up areas, the segmentation results have shown that the segmented image pixels are significantly fragmented [25]. However, the current studies on the optimization of image segmentation results are fewer, and more attention is paid to how to use different segmentation methods to segment images [26].

As a kind of urban geographic big data, POI data can reflect the different functional attributes of an area within an urban city through the degree of spatial distribution of data [27]. Moreover, the agglomeration of POI data in urban spaces has a strong spatial correlation with the distribution of the high and low values of NTL data [28], that is, NTL data could distinguish areas with different development levels in an urban space through the distribution of high and low NTL values [29], while POI data could reflect different urban functions and infrastructure distribution through quantitative agglomeration [30]. Additionally, with the rapid development of cities, the internal spatial information is increasingly complex, and it is increasingly difficult for single data to reflect such complex spatial information [31,32]. Therefore, researchers try to fuse POI data with NTL data to improve the feedback and observation ability of urban spatial information [33,34]. At present, although the study on the fusion of POI data and NTL data in urban areas has achieved good results, the current fusion of two kinds of data is mainly the elimination the spatial outliers in NTL data by using POI data to improve the observation accuracy of NTL data. Such fusion mainly focuses on NTL data, and the value of POI and other big data has not been fully reflected [35,36].

In general, the current study on data fusion and the extraction of urban built-up areas may have the following study insufficiencies: Firstly, from the perspective of the study area, too much attention is paid to cities with a high development level and large built-up areas, and less attention is paid to small and medium-sized cities that are still in rapid development [37]. Secondly, from the perspective of study methods, the effects of different methods, especially image segmentation methods, on NTL data extraction of built-up areas have been more discussed, and the results obtained by different segmentation methods have not been further optimized [38]. Thirdly, from the perspective of study data, although there have been many studies on the fusion of POI data and NTL data, image modification based on NTL data has not maximized the role of POI data [39]. Therefore, the contribution of this study was mainly reflected in the following aspects: First, from the study area, this study selected the non-first-tier cities with the highest average growth rate of urban built-up areas in China over the past ten years. Second, from the study methods, this study supplemented the optimization of image pixels after image segmentation. Third, from the study data, the pixel-level fusion of NTL data and POI data was performed by a feasible method in this study, which realized the fusion of NTL data and POI data at the same level.

A new method for urban built-up area extraction is proposed in this study, which could enrich the theoretical study of urban space. It is also believed that the accurate extraction of Zhengzhou's urban built-up area would undoubtedly contribute to the accurate judgment of urbanization in Zhengzhou, thus providing a theoretical foundation for regional governance and policymaking regarding the harmonious urban–rural development of Zhengzhou.

## 2. Materials and Methods

### *2.1. Study Area*

With the rapid urbanization of China, the expansion of built-up areas in China has become more obvious. In order to better test the extraction effect of built-up areas, this study selected Zhengzhou, where urban built-up areas have been expanding rapidly in the past decade, rather than first-tier cities such as Beijing, Shanghai and Guangzhou as the study area. In Zhengzhou, as the capital city of Henan Province (Figure 1), according to data statistics, the growth rate of the built-up areas in Zhengzhou has generally exceeded 120% in the past decade, and more than 130% in 2020 and 2021; such a growth trend is unique in China [40]. With the rapid development of built-up areas, the accurate extraction of built-up areas has become an important prerequisite for formulating urban development plans. Through the case analysis of Zhengzhou, this study discusses the extraction of built-up areas under high-speed changes, which not only has important practical guiding significance for the urban development and urban-rural planning of Zhengzhou during the rapid development period but also plays a positive role in the extraction of other urban built-up areas with less change.

The study area of this study mainly consisted of 8 administrative districts in Zhengzhou: Jinshui District, Zhongyuan District, Guancheng District, Erqi District, Huiji District, Shangjie District, Xinzheng District and Xingyang District.

### *2.2. Study Data*

The study data used in this study were mainly the Luojia-01 NTL data and POI data.

The Luojia-01 data, provided by the Luojia-01 experimental satellite, can be downloaded for free at http://59.175.109.173:8888/Index.html (accessed on 1 January 2022). Compared with the DMSP/OLS and NPP/VIIRS NTL data, the Luojia-01 NTL data have a resolution of 130 m and a width of 20 km, which enables Luojia-01 NTL data to be more perfect in spatial scale analysis [41]. Additionally, the finer numeric features of the NTL data greatly improve its extraction accuracy within urban spaces. The specific technical indicators of Luojia-01 are as follows: the waveband is from 0.5 to 0.9 μm, the wavelength is from 480 to 800, the spatial resolution is from 100 to 150 m, the illumination is 10 lux, the orbit type is a sun-synchronous circular orbit, the orbit standard altitude is from 500 to

600 km and the observation period is 15 days. The NTL data of Zhengzhou from October 2018 to October 2021 were obtained for this study after accessing the website mentioned above. Due to the discontinuity, unsaturation and it being easily affected by laser and fire of the NTL data, the NTL values are prone to generate negative values and outliers. Therefore, this study used radiometric calibration to modify the NTL data [42]. Thanks to the daytime and nighttime imaging capabilities of the Luojia-01 NTL data, the non-uniformity calibration of each pixel of the noctilucent sensor was realized by constructing a day–night radiation reference transfer model. Specifically, the calibration model was solved by using daytime imaging images, and then the influence of nighttime light was modified and compensated, that is, the low-gain relative correction coefficient of the sensor pixels calibrated in the daytime was converted to the high-gain relative correction parameter in the nighttime based on this model [43]. The corrected NTL data are shown in Figure 2.

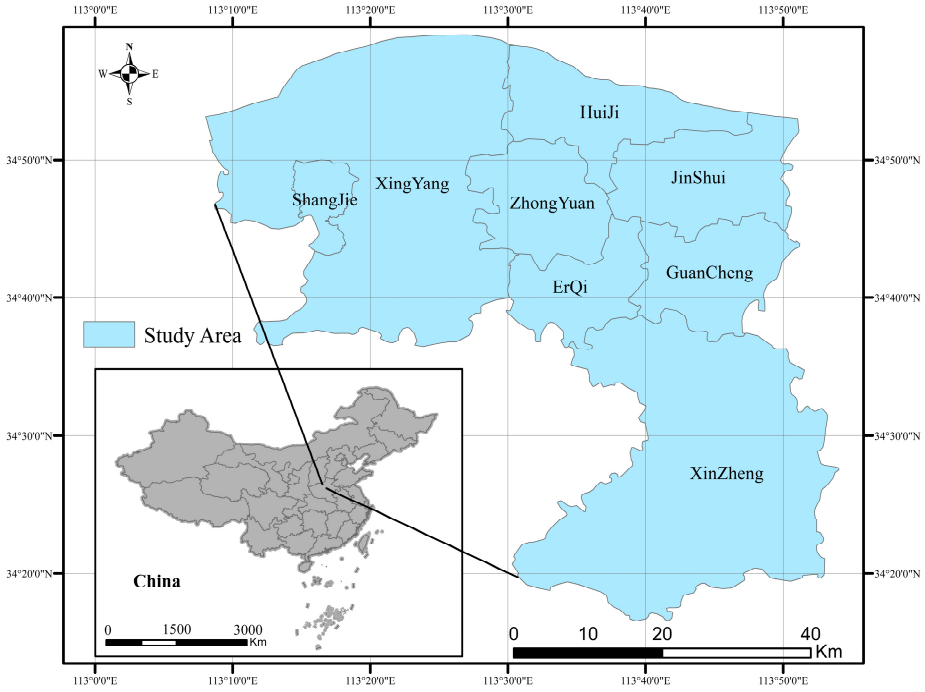


**Figure 1.** Study area.

POI data refer to the point dataset in a networking electronic map, which consists of four attributes: name, address, coordinate and category [44]. At present, numerous map companies, such as Baidu Maps, Amap and QQ Maps, have provided developers with API (application programming interface) access services, which allow users to sense all kinds of reasonable data. A POI can represent a shop, a building or a node in a building in the geographic information system (GIS). Therefore, a POI point may have multiple functions, so in order to prevent the POI point with multiple functions from interfering with the final analysis, this study filtered and cleaned the acquired POI data through the location and semantic constraints of the POI [45]. By accessing the API provided by Amap (www.amap.com (accessed on 1 January 2022)), this study sourced POI data from Zhengzhou in December 2021, and the category and quantity of POI data were 22 and 669,213, respectively. After screening, duplicate checking, filtering and cleaning all the obtained POI data, the category and quantity were 16 and 459,817, respectively. Since the spatial resolution of the NTL data used in this study was 130 m, this study used a 130 m spatial grid to count the number of POIs to unify the spatial resolution of the data. The number and spatial distribution of POI in Zhengzhou are shown in Figure 3.

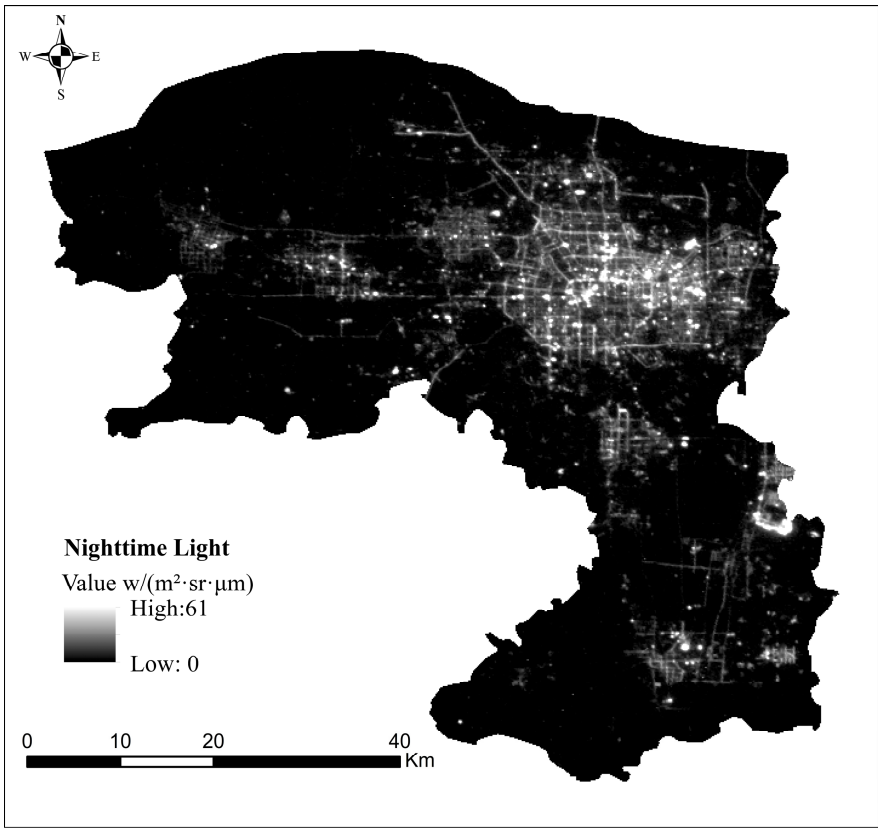


**Figure 2.** Preprocessing results of Zhengzhou NTL data.

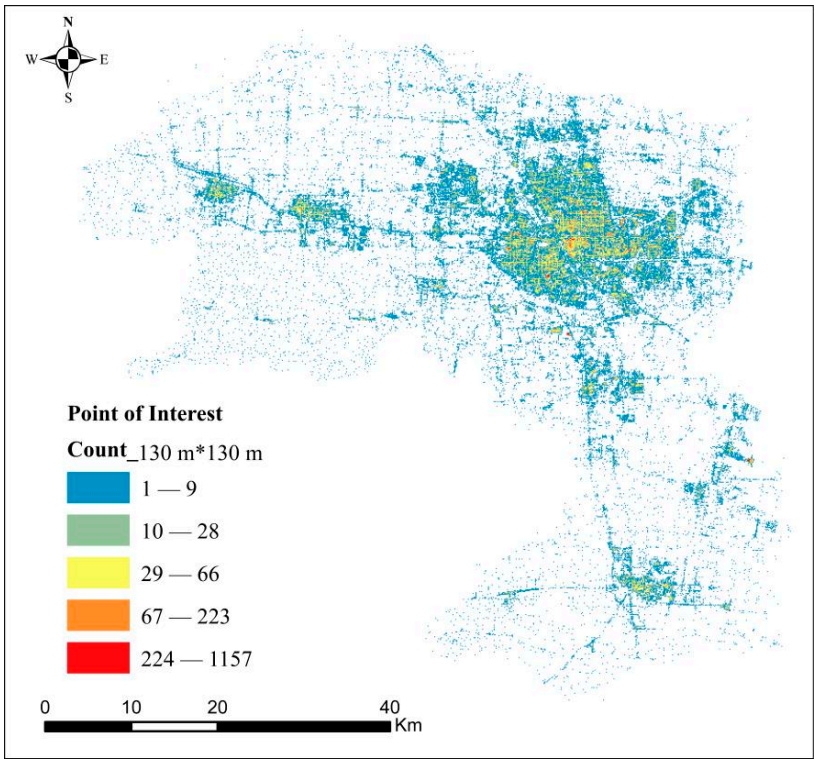


**Figure 3.** The quantity and spatial distribution of POI data in Zhengzhou.

### 2.3. Methods

The method flow chart of built-up area extraction is shown in Figure 4.

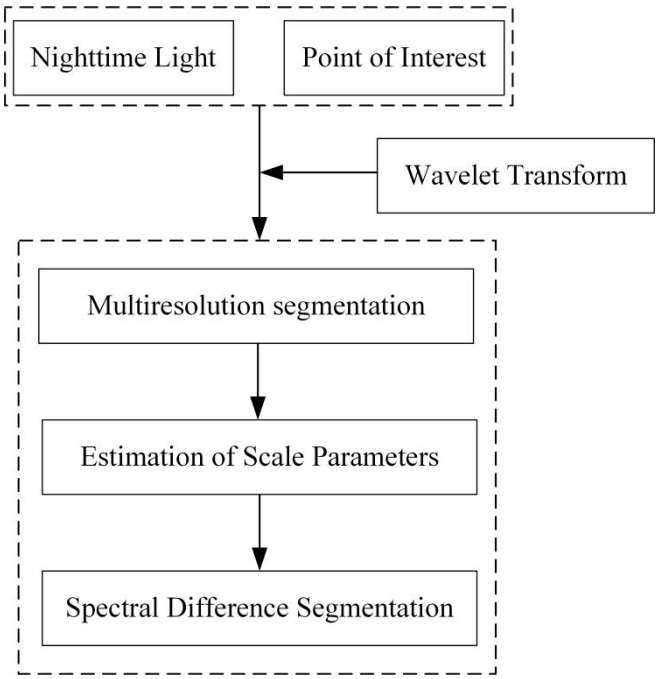


**Figure 4.** Framework of study methods.

The study idea of this study is as follows: Firstly, the NTL data were used to extract urban built-up areas through multi-resolution segmentation, estimation of scale parameters and spectral difference segmentation. Then, the built-up areas were extracted by the above methods through the fusion of POI data and the NTL data, and the results of the extraction of urban built-up areas before and after the fusion of the NTL data and POI data were further compared. A single point of POI data is not suitable for extracting urban built-up areas, the main reason being that the urban built-up areas extracted from POI data are too different from the actual urban built-up areas, so they are not comparable [38,39]. Therefore, this study only compared and analyzed the fusion results of POI data and the NTL data.

#### 2.3.1. Wavelet Transform (WT)

As an important branch of information fusion, the purpose of image fusion is to synthesize the multi-band information of a single sensor or the information provided by different types of sensors, thereby eliminating the redundancy and contradiction that may exist between the multi-sensor information so as to enhance the transparency of the information in the image and improve the accuracy, reliability and usage of image interpretation, thus resulting in a clear, complete and accurate information description of the target [46–48]. At present, image fusion includes data-level fusion, feature-level fusion and decision-level fusion, among which data-level fusion, also known as pixel-level fusion, refers to the process of directly processing the data collected by sensors to obtain the fused image, which is one of the focuses of the current image fusion study [49]. The advantage of data-level fusion is to retain as much raw field data as possible while providing subtle information that other fusion levels cannot provide. There are spatial domain algorithms and transform domain algorithms in data-level fusion, among which the wavelet transform is the most important and commonly used method to cover both spatial and temporal domains [50].

As a global-scale transformation, *WT* is a pixel-based image fusion algorithm [51]. Compared with other fusion algorithms, *WT* has a better station-keeping ability in both the time domain and the frequency by providing a dynamic "time-frequency window" [52].

Through this window, *WT* can fully consider the interactive relationship between the time domain and frequency of an image, which makes *WT* an ideal tool for image fusion [53]. The formula of *WT* is as follows:

$$WT(\alpha,\tau) = f(t)\varphi(t) = \frac{1}{\sqrt{\alpha}} f(t) \int_{-\infty}^{+\infty} \varphi\left(\frac{t-b}{\alpha}\right) dt \quad (1)$$

where $f$ is the signal vector, $t$ is the basic wavelet function, $\alpha$ is the scale, $\tau$ is the translation and $b$ is the parameter.

Regarding the principle of *WT*, the original image that needed to be fused was decomposed, and then the high- and low-frequency components of the image in different directions (horizontal direction, vertical direction and diagonal-edge direction) were obtained. The high- and low-frequency components contained all the detailed parts of the original image with different details corresponding to the different features of the image. Then, the detailed information of different images was compared in the dynamic window of *WT*, after which fusion was realized by setting the maximum absolute value within the *WT* domain as the most appropriate scale. Finally, the image was obtained after inverse transformation was conducted on the fused image. The fusion process of the wavelet transform is shown in Figure 5.

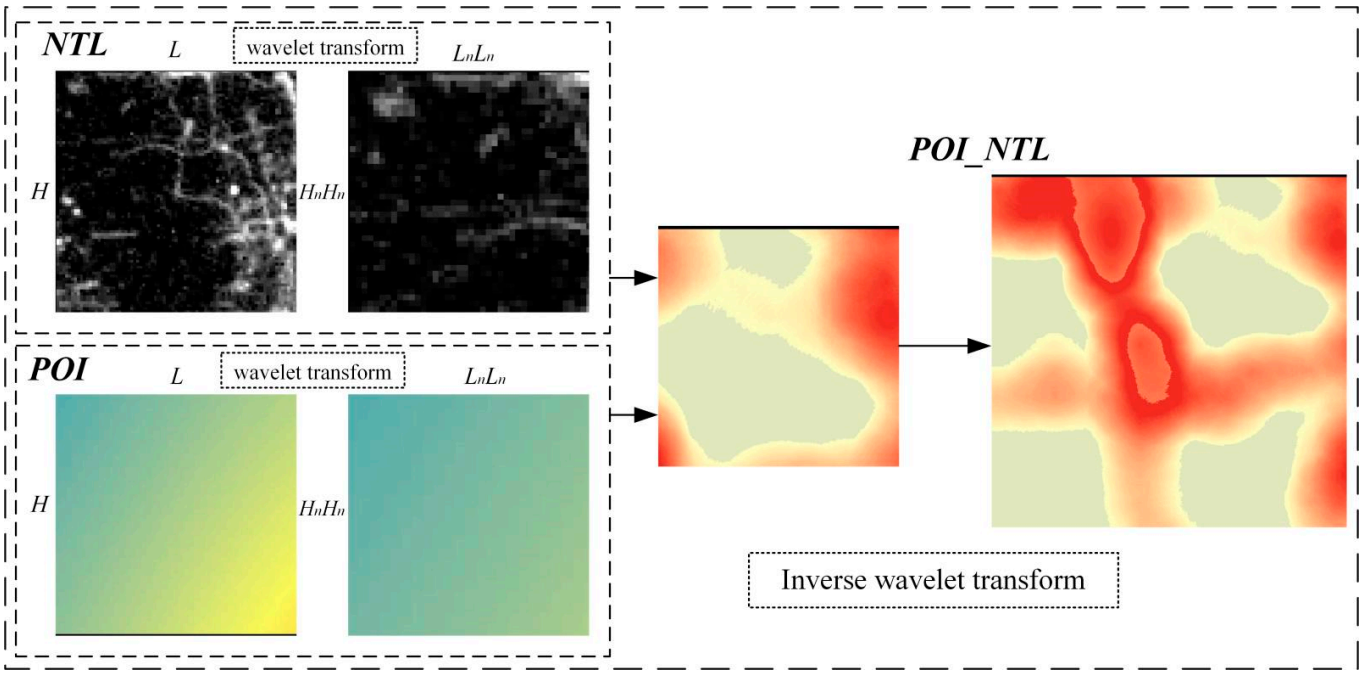


**Figure 5.** Principle of wavelet transform.

### 2.3.2. Multiresolution Segmentation

Although image segmentation is one of the most widely used methods of interpreting high-resolution remote-sensing images, the methods of image segmentation include threshold-based segmentation, region-based segmentation, edge-based segmentation and segmentation based on specific theories. As the rich spatial structure information and geographical feature information in remote-sensing images have different performances at different scales, multi-resolution segmentation is considered as a reliable method and is widely used in image segmentation at present [54]. As an object-oriented bottom-up image segmentation algorithm, multiresolution segmentation differs from other algorithms in the way of segmenting images. Multiresolution segmentation can segment a target image by merging adjacent elements on the premise of ensuring the maximum average intersegment heterogeneity and maximum intersegment homogeneity [55].

There are three main factors of multiresolution segmentation: scale, shape and tightness. After segmentation with the selected proportion parameters, the average value and the area of all the segmented images can be calculated. Then, the weighted mean variance after segmentation can also be calculated, and only when the variance reaches the maximum value is the scaling factor the most appropriate.

$$C_k = \frac{1}{n}\sum_{i=1}^{n} C_{ki} \tag{2}$$

$$\overline{C}_k = \frac{1}{m}\sum_{k=1}^{m} C_k \tag{3}$$

$$S^2 = \frac{1}{m}\sum_{k=1}^{m} \left(\overline{C}_k - \overline{C}\right)^2 \tag{4}$$

where, $C_k$ is the average luminance of a single image object in $k$th band, $n$ is the number of pixels in a segmented image, $\overline{C}_k$ is the average luminance of all objects in the image in the $k$th band, $\overline{C}_{ki}$ is the DN value of the $i$th pixel of segment $k$, $m$ is the total number of images after segmentation and $S^2$ is the weighted mean variance of the DN values of images after segmentation.

2.3.3. Estimation of Scale Parameters (ESP)

ESP is used to optimize segmentation results thanks to its full use of multiple bands characteristic of remote sensing, which results in a connection between the estimation of segmentation results and process. The local variance of different objects within one band is first calculated, and then the mean value of the local variance within multiple bands is calculated to optimize the segmentation results.

$$meanLV = (LV_1 + LV_2 + \ldots\ldots LV_n) \tag{5}$$

where $LV$ is the local variance and $LV_n$ is the local variance of an object within one band.

When the interior homogeneity of one object reaches its maximum value, the differences among objects are the largest, and the largest scale of local variance is defined as the optimal segmentation scale.

2.3.4. Spectral Difference Segmentation (SDS)

As a segmentation optimization method, SDS assists with the promotion of the fragmentation of segmented images after merging based on multiresolution segmentation and ESP, contributing to a higher generalization of image segmentation. The formula for SDS after normalizing the weights of bands is as follows:

$$S_{diff} = \frac{\sum_k w_k}{w}\left(\frac{1}{n}\sum_n b_n - \frac{1}{m}\sum_m b_m\right) \tag{6}$$

where $S_{diff}$ is the spectral difference value between adjacent objects; $k$ is the number of bands; $w_k$ is the weight of the $k$th band; $w$ is the sum of all band weights; $n$ and $m$ are the sums of pixels within adjacent objects; and $b_n$ and $b_m$ are the gray values of the $n$ pixel and $m$ pixel within adjacent objects, respectively. $S_{diff}$ is the only parameter of the SDS algorithm; the larger the value is, the easier the merging of adjacent objects.

## 3. Results

### *3.1. Urban Built-Up Area of Zhengzhou Extracted by Different Data*

3.1.1. Urban Built-Up Area of Zhengzhou Extracted by NTL Data

As a segmentation optimization method, SDS assists with the promotion of the fragmentation of segmented images after merging based on multiresolution segmentation and ESP, contributing to a higher generalization of image segmentation. The formula for SDS after normalizing the weights of bands is as follows:

As shown in the preprocessing result of the NTL data (Figure 2), the high NTL values were mainly concentrated in Jinshui District, Zhengzhou railway station of Erqi District, the college town of Zhongyuan District, the Zijingshan trading area of Guancheng District and Xinzheng International Airport, while the NTL values in other districts were relatively lower. Therefore, it can be seen from the distribution of the high and low NTL values that there was a significant spatial difference in the urbanization development of Zhengzhou, with Zhongyuan District, Jinshui District and Erqi District playing the central role in Zhengzhou, while the other areas, including Guancheng District and Xinzheng International Airport were mainly concentrated with lower NTL values since these areas are located at a long distance from the urban center [56].

In this study, multiresolution segmentation was first used to segment the NTL data to extract the urban built-up area of Zhengzhou. Then, the scale parameters of multiresolution segmentation were determined to be 9, 0.4 and 0.7 by ESP, and the urban built-up area extracted by determining the scale parameters was finally obtained, as shown in Figure 6. Figure 6 shows that the urban built-up area extracted by the NTL data mainly had the following features. First, the area extracted by the NTL data was 623.45 square kilometers, accounting for 80.66% of the whole urban area of 772.92 square kilometers. Second, although the extracted built-up area was mainly concentrated in Erqi District, Guancheng District, Zhongyuan District and Jinshui District, there were still built-up clusters in both Xingyang and Xinzheng. Third, from the perspective of the extracted built-up areas, there were too many patches that resulted in the severe fragmentation of the extracted built-up areas. Additionally, there were obvious urban void phenomena in Zhongyuan District and Xingyang with more complex boundaries. Moreover, the main roads around Xinzheng International Airport were all extracted as urban built-up areas by the NTL data. Generally, the method of extracting urban built-up areas by single-source NTL data is ineffective, which calls for subsequent studies to perfect the method.

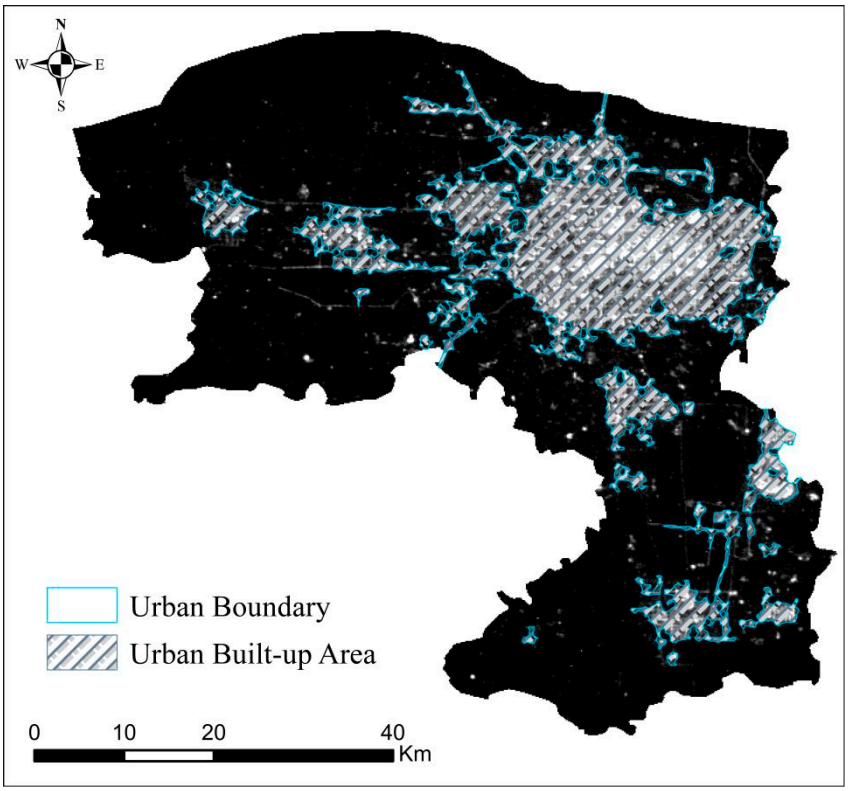


**Figure 6.** Urban built-up area of Zhengzhou extracted by NTL data.

3.1.2. Urban Built-Up Area of Zhengzhou Extracted by Fusing NTL and POI Data

There is a deep connection between the distribution of POI data and urban function; that is, the more concentrated the POI data are, the stronger the urban function will be. The number and spatial distribution of POI data in Zhengzhou are shown in Figure 3. There was a significant spatial difference in the POI data between the built-up areas and non-built-up areas, with the POI data mainly concentrated in Erqi District, Zhongyuan District, Jinshui District, Guancheng District and Xinzheng. By comparing the POI data to the NTL data, the number and spatial distribution of POI data in Zhengzhou were similar to those of the NTL data, which meant that the POI data and NTL data could be fused.

*WT* was used in this study to fuse the POI data and NTL data. First, this study used *WT* to segment the POI data and NTL data. Second, the wavelet coefficients of different bands were compared since the wavelet coefficients corresponded to different feature parts of the image, so it was necessary to keep the absolute value of the wavelet coefficients at the maximum in the *WT* domain of different frequency bands. Third, inverse transformation was conducted after fusing the POI data and NTL data by setting appropriate wavelet coefficients. The image after data fusion is shown in Figure 7. Figure 7 shows that after data fusion, there was a more obvious spatial distribution between the high and low values of the fused POI_NTL data, with high values mainly concentrated in Jinshui District, Zhengzhou railway station in Erqi District, the central trading area of Guancheng District and the urban city of Xinzheng, while the areas with higher values, such as Xinzheng International Airport and Xingyang, were where lower values were mainly concentrated.

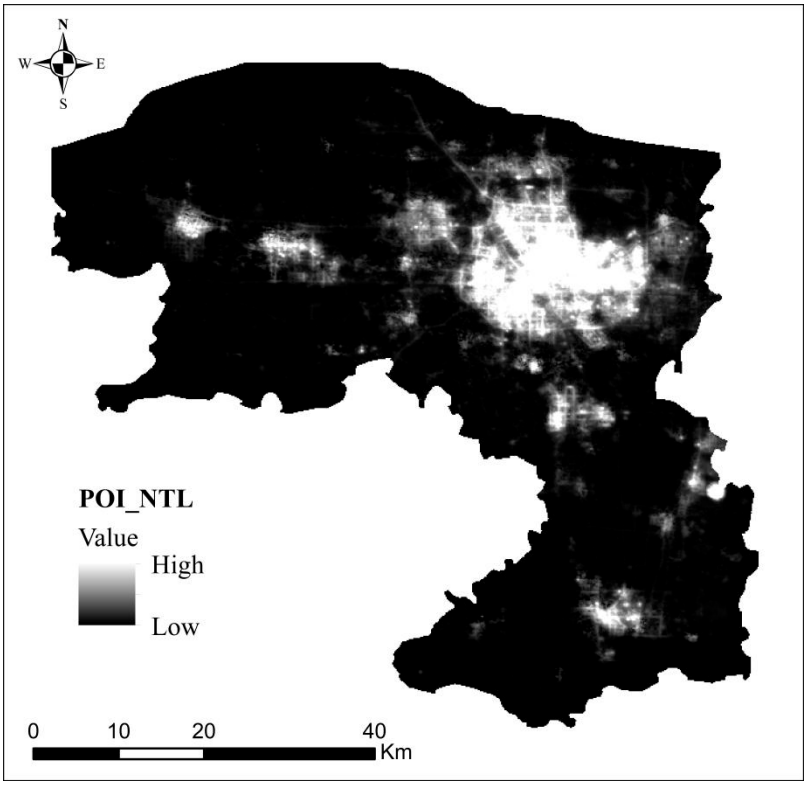


**Figure 7.** Data fusion results after fusing POI and NTL data.

Then, multiresolution segmentation was used in this study to extract the urban built-up area in Zhengzhou by the fused POI_NTL data with segment parameters determined by EPS values of 10, 0.5 and 0.5, and the urban built-up area was extracted after data fusion was finally obtained, as shown in Figure 8. Figure 8 shows that the urban built-up area had the following features. First, the area extracted after data fusion was 661.54 square kilometers, accounting for 85.58% of the whole built-up area. Second, only five city clusters were extracted, concentrated at the junction of Erqi District and Jinshui District as well as

Shangjie district, Xingyang and the urban city of Xinzheng. Third, compared with the urban built-up area extracted by the NTL data, there were fewer urban patches that were extracted after data fusion, which contributed to the modification of the fragmentation phenomenon within the urban built-up area. Additionally, there were no more obvious urban voids. In particular, no clusters around Xinzheng International Airport were extracted. In general, the fused POI_NTL data improved the extraction accuracy to a certain degree.

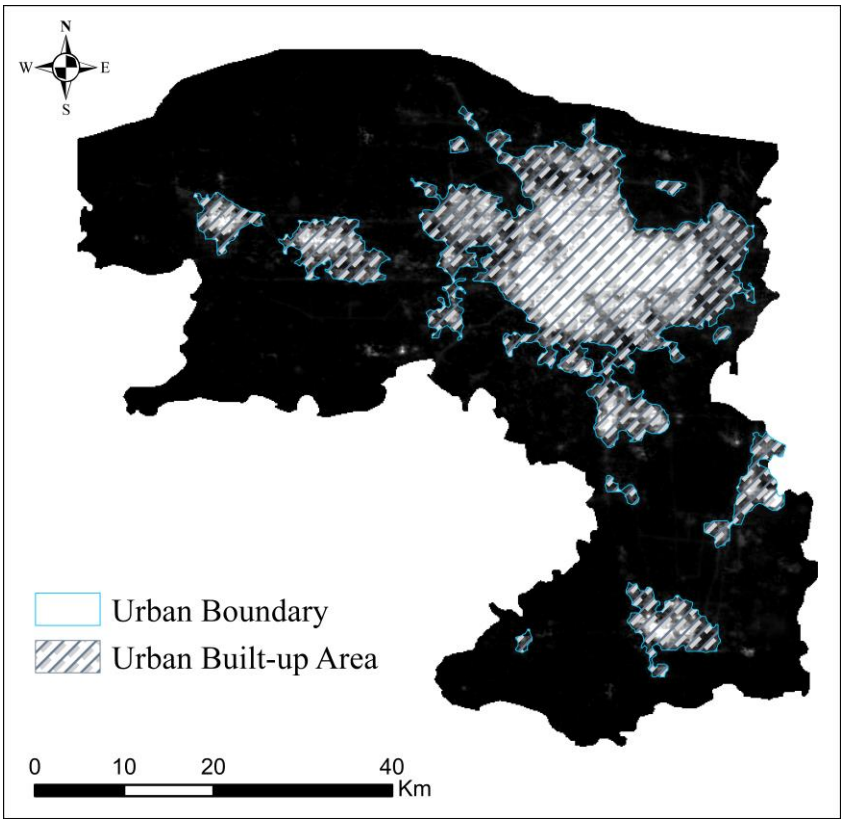


**Figure 8.** Urban built-up area of Zhengzhou extracted by POI_NTL data.

### *3.2. Comparative Verification of the Extraction Results*

#### 3.2.1. Comparative Analysis before and after Data Fusion

By comparing the NTL data to the fused POI_NTL data, as shown in Figure 9, there was a similarity in the macroscale between the NTL data and POI_NTL data, which could directly represent the urban internal spatial structure. Additionally, the high and low values of both sets of data all showed a downward trend from urban areas to rural areas. Therefore, it can be concluded that after data fusion, the fused POI_NTL data could more accurately represent the urban internal spatial structure by retaining the features of the NTL data while enlarging the characteristics of the POI data.

By constantly comparing the NTL data to the fused POI_NTL data at the microscale, it was found that there was a distortion resulting from the single attribute of NTL data taking nighttime light brightness as the only criterion to extract the build-up area. As shown in Figure 9, on the one hand, there was little nighttime light captured by the NTL data in the residential communities and central business district (CBD) of Zhengzhou, which led to the extraction of "light voids" within the urban built-up area. After data fusion, the POI_NTL data fully combined the advantage of the POI data with that of the NTL data by taking the distribution of the POI data in residential communities and CBD areas into account, which made up for the deficiency of the NTL data in extracting urban built-up areas, contributing to the stronger spatial integrity of the extracted built-up areas. On the other hand, a large amount of nighttime light was generated at Xinzheng International Airport and around the main roads, which led to high NTL concentrations [37]. However,

there were no corresponding high values of the POI data in these regions, especially around the main roads. In the altered regions around Xinzheng International Airport and around the main roads, there were no obvious high values identified by the fused POI_NTL data, which was more in line with the actual situation of Zhengzhou.

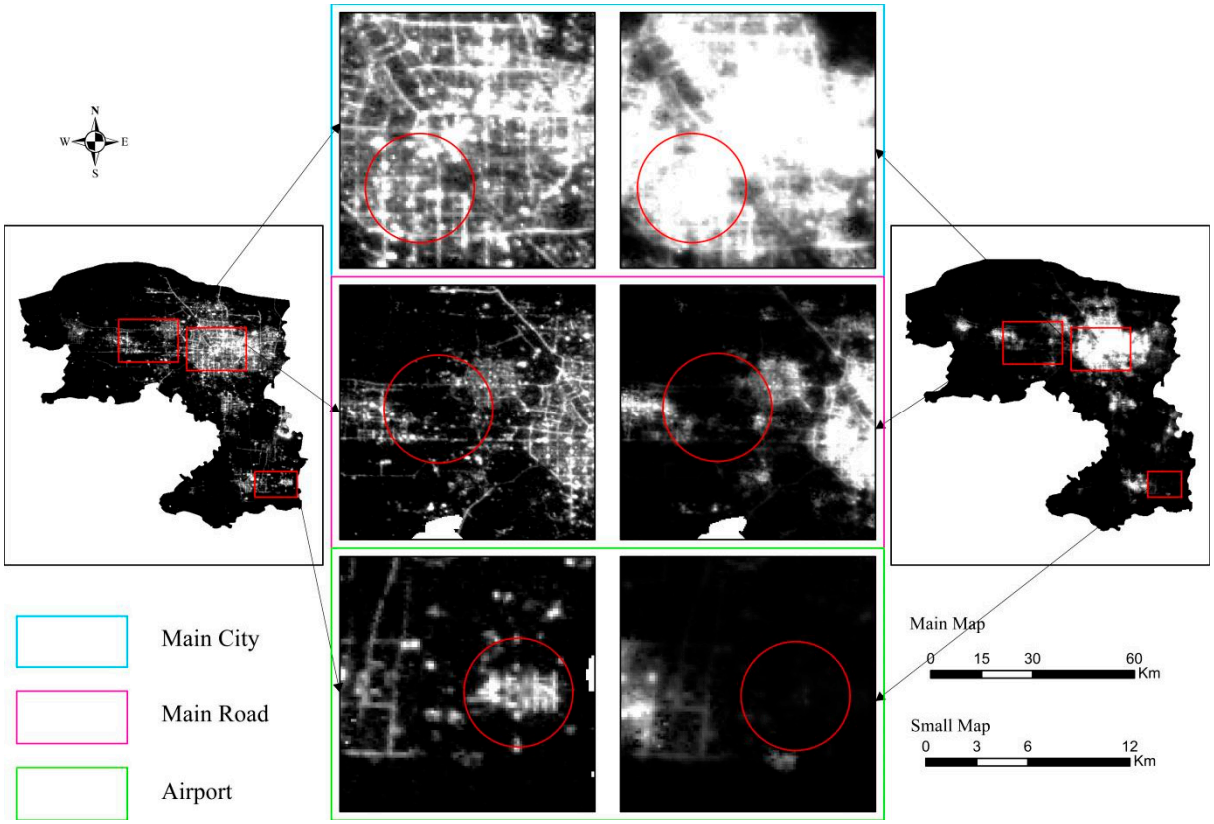


**Figure 9.** Comparative analysis before and after data fusion.

Generally, although the urban internal spatial structure could be represented, the urban built-up area could be attracted by the NTL data, and there was a distortion phenomenon resulting from the only attribute of the NTL data. The POI data could represent the number of structures within urban cities by showing the number and spatial distribution of the POI data. At the same time, the actual function of urban cities could also be reflected by the agglomeration degree of the POI data. Therefore, the fusion of the NTL data with the POI data could undoubtedly modify the distribution phenomenon generated by the NTL data, thus greatly improving the extraction accuracy.

#### 3.2.2. Comparative Analysis of Extracted Urban Built-Up Areas before and after Data Fusion

As shown in Figure 10, the area of the urban built-up area extracted by the POI data and the fused POI_NTL data were 623.45 square kilometers and 661.54 square kilometers, accounting for 80.66% and 85.58% of the total built-up area, respectively. From the area extracted by these two sets of data, it was found that although there were no significant differences, the 5% improvement achieved by the fused POI_NTL data still proved that the utilization of multiresolution segmentation was of great help in image segmentation.

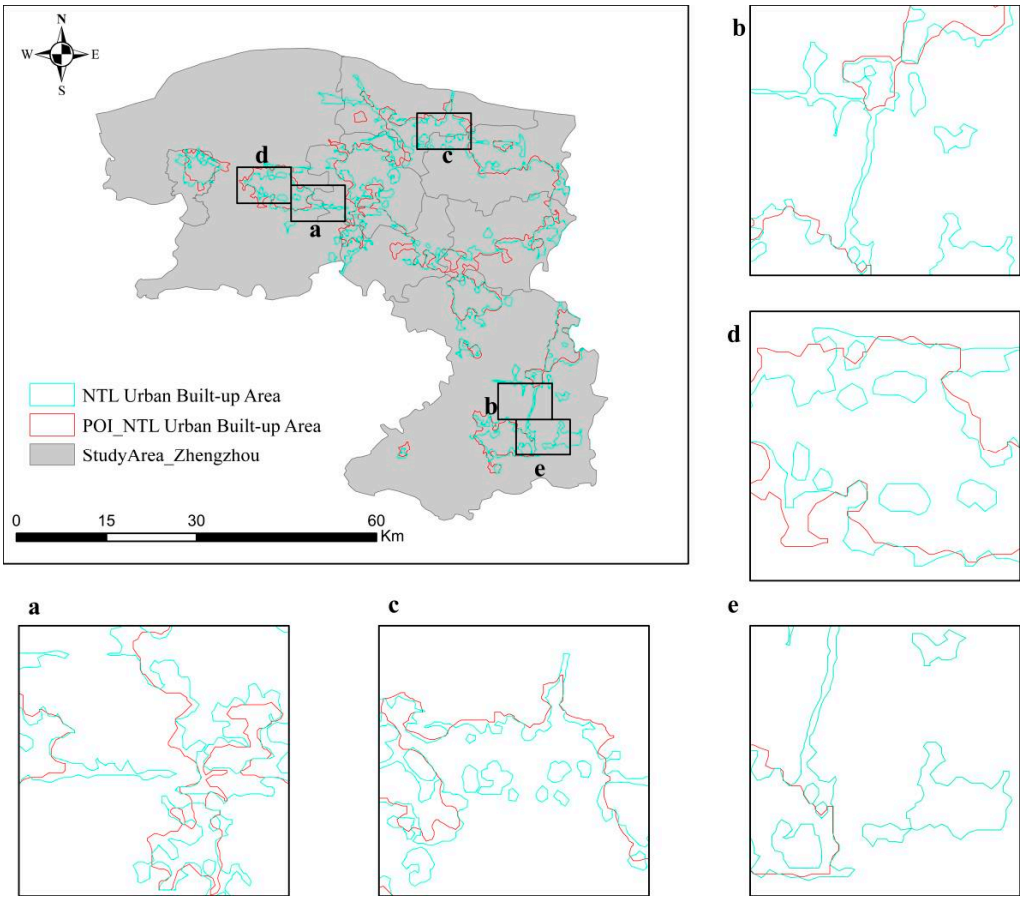


**Figure 10.** Comparison of urban built-up areas extracted by NTL data and POI_NTL data.

After comparing the urban built-up area extracted by the NTL data to that extracted by the POI_NTL data, it was found that there were many urban voids in the built-up area extracted by the NTL data with more complex boundary details. Additionally, the differences in nighttime light resulted in unsatisfactory results among different urban built-up patches by extracting non-built-up areas with high nighttime light values as built-up areas. The fused POI_NTL data greatly improved the extraction accuracy. For example, as seen in Figure 10a,b, there were many road clusters identified by the NTL data to be built-up areas, which was in contrast to those identified by the POI_NTL data. Second, there were large numbers of light voids in the built-up area extracted by the NTL data, which did not confirm the actual results. The built-up area extracted by the POI_NTL data greatly modified this situation and had more complete boundary details. Additionally, the urban clusters, which were identified by NTL data near Xinzheng International Airport and around main roads as built-up areas, were identified as non-built-up areas by the POI_NTL data, which was more consistent with reality.

Generally, although urban built-up areas could be extracted by both the NTL data and the POI_NTL data, there was a severe fragmentation phenomenon in the built-up areas extracted by the NTL data since the NTL data failed to consider the actual development of Zhengzhou. The area extracted by the POI_NTL data not only made up for the deficiency of that extracted by the NTL data but also enriched the details of the extracted built-up area, which was more in line with reality.

#### 3.2.3. Precision Verification

A total of 3000 random pixels in Zhengzhou were selected to verify the built-up area extracted in this study, of which 1000 pixels were training data and 2000 pixels were verification data. After conducting field visits with the help of Google Earth high-resolution

image data, all 3000 pixels were verified to be located within the built-up area of Zhengzhou. The confusion matrix obtained according to the verification results is shown in Table 1. The precision in Table 1 is the proportion of all the pixels that were successfully verified. While the kappa coefficient was used to verify classification precision to further track consistency, the possible values of the kappa coefficient ranged from −1 to 1; the closer the value was to 1, the better the extraction was.

**Table 1.** Precision verification.

| Data | | Urban | Rural | Accuracy | Kappa |
|---|---|---|---|---|---|
| NTL | Urban | 498 | 70 | 85.95% | 0.7089 |
| | Rural | 211 | 1221 | | |
| POI_NTL | Urban | 532 | 36 | 96.15% | 0.8454 |
| | Rural | 101 | 1331 | | |

In Table 1, the values in the urban areas and rural areas represent the number of the 2000 random verification points that fell into the extracted built-up areas and non-built-up areas, namely the number of points that were successfully verified. Accuracy represents the ratio of the number of points that were successfully verified to the total number.

As seen from Table 1, the precision of the built-up area extracted by the NTL data and POI_NTL data were 85.95% and 96.15%, with kappa coefficients of 0.7089 and 0.8454, respectively. From the extraction precision and kappa coefficients, the extraction effect obtained by the fused POI_NTL data had an edge over that obtained by the single-source NTL data. After data fusion, the deficiency of single-source data extraction was compensated for, and the internal spatial structure extracted was more integrous [57].

## 4. Discussion

Although NTL data are one of the commonly used types of data in urban-related studies, the deficiency of NTL data leads to large errors in the study results of urban interior spaces. Moreover, there is light overflow and oversaturation in NTL data [58,59]. Therefore, researchers have begun to try to fuse POI data to improve the accuracy of NTL data in urban space on the basis of considering the strong spatial correlation between POI data and NTL data in urban space. This study used a wavelet transform to fuse NTL data and POI data to extract urban built-up areas. The results showed that the extraction accuracy after data fusion reached 96.15%, which was a great improvement compared with the accuracy of extracting urban built-up areas by the single-source NTL data [60]. Although the NTL data could fully reflect the development gap of cities, further supplementing the POI data on the basis of this difference could make it more accurate in extracting urban built-up areas. Compared with existing studies on the fusion of the NTL and POI data, this study improved the accuracy of the threshold segmentation of different data by using the ESP SDS algorithm on the basis of multiresolution segmentation, and the segmentation accuracy of the single-source NTL data reached 85.95%, fully demonstrating the accuracy of this study method.

The traditional extraction and division of urban built-up areas mainly depends on the subjective will of the government or the use of socioeconomic and statistical data [61,62]. The extensive application of remote-sensing data represented by NTL has made the extraction of urban built-up areas gradually move toward quantitative analysis. However, NTL data can only judge whether a certain area is an urban area simply by capturing the nighttime light brightness generated by urban infrastructure, which ignores the actual social development of urban space [63]. This study fused POI data that can represent the development of urban functions with NTL data and then formed POI_NTL data that could accurately extract urban built-up areas, which comprehensively considered the relationship between urban infrastructure and urban development functions and gave a huge advantage in the process of extracting urban built-up areas [64].

However, there is no doubt that there were some limitations in this study. From the Luojia-01 data used in the study, firstly, compared with the observation period of the same type of NTL data, such as NPP-VIIRS, which is 12 h, the observation period of the Luojia-01NTL data is 15 days, which makes the monthly average method of Luojia-01NTL data vulnerable, such as cloud cover in the observation area [65]. Secondly, there are more and more cold white lights in cities, while the wavelength of Luojia-01NTL data ranges from 400 to 800 μm, making Luojia-01 unable to observe these cold white lights, which undoubtedly would have a certain impact on the results [66]. Finally, although the spatial resolution of Luojia-01 night light is higher than that of other NTL data, the time series segment provided by Luojia-01 is not conducive to long-term observation and study. Additionally, the development and change in urban built-up areas are dynamic, and the scope of urban built-up areas will change dramatically with the development of the city. Therefore, to better extract urban built-up areas and better serve urban planning and construction, it is necessary to extract the scope of urban built-up areas at different periods of time to analyze the relationship between the spatial changes in built-up areas and urban development and further propose better strategies and plans conducive to urban development.

Since NTL data are easily affected by sensors and human activities when used in cities, this study further used a wavelet transform to fuse the POI data to extract urban built-up areas on the basis of NTL data, which avoided the possible problems existing in the extraction of urban built-up areas from the single NTL data, thus minimizing the shortcomings of the single NTL data in extracting built-up areas. Although this study took Zhengzhou, China as a case study, the methodology of this study could be extended to the whole of China and even the world, because from a global perspective, both NTL data and POI data have certain limitations. The limitations of NTL data have been mentioned in the insufficiency part of the study, while the POI data provided by Chinese service providers do not cover global POI data, so this study was more about providing a data fusion idea for the study of extracting global urban built-up areas, and a lot of additional work is needed in the future process of extracting global urban built-up areas.

## 5. Conclusions

The accurate extraction of urban built-up areas is an important prerequisite for analyzing the urbanization process and judging the spatial relationship within urban cities. Based on the characteristics of NTL data and POI data, new POI_NTL data were obtained in this study by fusing NTL data and POI data. Then, by comparing the results of the urban built-up area extracted by the single-source NTL data and the fused POI_NTL data, the accuracy of the urban built-up area extracted by NTL data was 85.95% and the kappa coefficient was 0.7089, while the accuracy of that obtained by the fused POI_NTL data was 96.15%, with a kappa coefficient of 0.8454. Therefore, fusion with POI data could effectively eliminate the phenomenon of urban voids and boundary fragmentation caused by NTL data. Moreover, POI data supplement the impact of urban functions on built-up areas on the basis of urban infrastructure development, which significantly improve the accuracy of urban built-up area extraction.

In this study, NTL data and POI data were fused by a wavelet transform, which not only helped to extract more accurate urban built-up areas but also had important theoretical and practical significance for accurately judging the urbanization level and formulating urban spatial policy and development planning.

**Author Contributions:** Conceptualization, Yaping Chen; methodology, Jun Zhang; software, Jun Zhang; validation, Yaping Chen and Jun Zhang; formal analysis, Yaping Chen; investigation, Jun Zhang; resources, Jun Zhang; data curation, Yaping Chen; writing—original draft preparation, Yaping Chen; writing—review and editing, Yaping Chen; visualization, Jun Zhang. All authors have read and agreed to the published version of the manuscript.

**Funding:** This research received no external funding.

**Data Availability Statement:** Not applicable.

**Conflicts of Interest:** The authors declare no conflict of interest.

## References


1. Anasuya, B.; Swain, D.; Vinoj, V. Rapid urbanization and associated impacts on land surface temperature changes over Bhubaneswar Urban District, India. *Environ. Monit. Assess.* **2019**, *191*, 790. [CrossRef] [PubMed]
2. Trinder, J.; Liu, Q. Assessing environmental impacts of urban growth using remote sensing. *Geo-Spat. Inf. Sci.* **2020**, *23*, 20–39. [CrossRef]
3. Ejiagha, I.R.; Ahmed, M.R.; Hassan, Q.K.; Dewan, A.; Gupta, A.; Rangelova, E. Use of remote sensing in comprehending the influence of urban landscape's composition and configuration on land surface temperature at neighbourhood scale. *Remote Sens.* **2020**, *12*, 2508. [CrossRef]
4. Liang, X.; Liu, X.; Chen, G.; Leng, J.; Wen, Y.; Chen, G. Coupling fuzzy clustering and cellular automata based on local maxima of development potential to model urban emergence and expansion in economic development zones. *Int. J. Geogr. Inf. Sci.* **2020**, *34*, 1930–1952. [CrossRef]
5. Li, H.M.; Li, X.G.; Yang, X.Y.; Zhang, H. Analyzing the relationship between developed land area and nighttime light emissions of 36 Chinese cities. *Remote Sens.* **2019**, *11*, 10. [CrossRef]
6. Andrade-Núñez, M.J.; Aide, T.M. Built-up expansion between 2001 and 2011 in South America continues well beyond the cities. *Environ. Res. Lett.* **2018**, *13*, 084006. [CrossRef]
7. Kotharkar, R.; Bahadure, P. Achieving compact city form through density distribution: Case of Indian cities. *J. Urban Plan. Dev.* **2020**, *146*, 04019022. [CrossRef]
8. Shi, K.; Huang, C.; Yu, B.; Yin, B.; Huang, Y.; Wu, J. Evaluation of NPP-VIIRS night-time light composite data for extracting built-up urban areas. *Remote Sens. Lett.* **2014**, *5*, 358–366. [CrossRef]
9. Zheng, Y.; Tang, L.; Wang, H. An improved approach for monitoring urban built-up areas by combining NPP-VIIRS nighttime light, NDVI, NDWI, and NDBI. *J. Clean. Prod.* **2021**, *328*, 129488. [CrossRef]
10. Kotarba, A.Z.; Aleksandrowicz, S. Impervious surface detection with nighttime photography from the International Space Station. *Remote Sens. Environ.* **2016**, *176*, 295–307. [CrossRef]
11. Wang, Z.; Yang, S.; Wang, S.; Shen, Y. Monitoring evolving urban cluster systems using DMSP/OLS nighttime light data: A case study of the Yangtze River Delta region, China. *J. Appl. Remote Sens.* **2017**, *11*, 046029. [CrossRef]
12. Wang, R.; Wan, B.; Guo, Q.; Hu, M.; Zhou, S. Mapping regional urban extent using NPP-VIIRS DNB and MODIS NDVI data. *Remote Sens.* **2017**, *9*, 862. [CrossRef]
13. Yu, B.; Tang, M.; Wu, Q.; Yang, C.; Deng, S.; Shi, K.; Peng, C.; Wu, J.; Chen, Z. Urban built-up area extraction from log-transformed NPP-VIIRS nighttime light composite data. *IEEE Geosci. Remote Sens. Lett.* **2018**, *15*, 1279–1283. [CrossRef]
14. Li, F.; Yan, Q.; Zou, Y.; Liu, B. Extraction Accuracy of Urban Built-up Area Based on Nighttime Light Data and POI: A Case Study of Luojia 1-01 and NPP/VIIRS Nighttime Light Images. *Geomat. Inf. Sci. Wuhan Univ.* **2021**, *46*, 825–835.
15. Liu, X.; Ning, X.; Wang, H.; Wang, C.; Zhang, H.; Meng, J. A rapid and automated urban boundary extraction method based on nighttime light data in China. *Remote Sens.* **2019**, *11*, 1126. [CrossRef]
16. Li, F.; Yan, Q.; Bian, Z.; Liu, B.; Wu, Z. A POI and LST adjusted NTL urban index for urban built-up area extraction. *Sensors* **2020**, *20*, 2918. [CrossRef]
17. Xiao, P.; Wang, X.; Feng, X.; Zhang, X.; Yang, Y. Detecting China's urban expansion over the past three decades using nighttime light data. *IEEE J. Sel. Top. Appl. Earth Obs. Remote Sens.* **2014**, *7*, 4095–4106. [CrossRef]
18. Cao, Q.; Yu, D.; Georgescu, M.; Wu, J.; Wang, W. Impacts of future urban expansion on summer climate and heat-related human health in eastern China. *Environ. Int.* **2018**, *112*, 134–146. [CrossRef]
19. Zou, Y.; Peng, H.; Liu, G.; Yang, K.; Xie, Y.; Weng, Q. Monitoring Urban Clusters Expansion in the Middle Reaches of the Yangtze River, China, Using Time-Series Nighttime Light Images. *Remote Sens.* **2017**, *9*, 1007. [CrossRef]
20. Sharma, R.C.; Tateishi, R.; Hara, K.; Gharechelou, S.; Iizuka, K. Global mapping of urban built-up areas of year 2014 by combining MODIS multispectral data with VIIRS nighttime light data. *Int. J. Digit. Earth* **2016**, *9*, 1004–1020. [CrossRef]
21. Wang, Z.; Shrestha, R.M.; Román, M.O.; Kalb, V.L. NASA's Black Marble Multi-Angle Nighttime Lights Temporal Composites. *IEEE Geosci. Remote Sens. Lett.* **2022**, *19*, 2505105.
22. Lee, G.-B.; Lee, M.-J.; Lee, W.-K.; Park, J.-H.; Kim, T.-H. Shadow Detection Based on Regions of Light Sources for Object Extraction in Nighttime Video. *Sensors* **2017**, *17*, 659. [CrossRef]
23. Cai, J.; Huang, B.; Song, Y. Using multi-source geospatial big data to identify the structure of polycentric cities. *Remote Sens. Environ.* **2017**, *202*, 210–221. [CrossRef]
24. Zhuo, L.; Zhang, C.; Zhu, X.; Huang, T.; Hu, Y.; Tao, H. iSEAM: Improving the Blooming Effect Adjustment for DMSP-OLS Nighttime Light Images by Considering Spatial Heterogeneity of Blooming Distance. *IEEE J. Sel. Top. Appl. Earth Obs. Remote Sens.* **2021**, *14*, 3903–3913. [CrossRef]
25. Hasan, S.; Shi, W.; Zhu, X.; Abbas, S. Monitoring of Land Use/Land Cover and Socioeconomic Changes in South China over the Last Three Decades Using Landsat and Nighttime Light Data. *Remote Sens.* **2019**, *11*, 1658. [CrossRef]

26. Bell, A.; Mantecon, T.; Diaz, C.; Del-Blanco, C.R.; Jaureguizar, F.; Garcia, N. A Novel System for Nighttime Vehicle Detection Based on Foveal Classifiers With Real-Time Performance. *IEEE Trans. Intell. Transp. Syst.* **2021**, *23*, 5421–5433. [CrossRef]
27. Zhang, J.; Zhang, X.; Tan, X.; Yuan, X. Extraction of Urban Built-Up Area Based on Deep Learning and Multi-Sources Data Fusion—The Application of an Emerging Technology in Urban Planning. *Land* **2022**, *11*, 1212. [CrossRef]
28. Zhang, S.; Wei, H. Identification of Urban Agglomeration Spatial Range Based on Social and Remote-Sensing Data—For Evaluating Development Level of Urban Agglomeration. *ISPRS Int. J. Geo-Inf.* **2022**, *11*, 456. [CrossRef]
29. Zhang, Q.; Seto, K.C. Mapping urbanization dynamics at regional and global scales using multi-temporal DMSP/OLS nighttime light data. *Remote Sens. Environ.* **2011**, *115*, 2320–2329. [CrossRef]
30. Chen, Y.; Deng, A. Using POI Data and Baidu Migration Big Data to Modify Nighttime Light Data to Identify Urban and Rural Area. *IEEE Access* **2022**, *10*, 93513–93524. [CrossRef]
31. Zhou, Y.; He, X.; Zhu, Y. Identification and Evaluation of the Polycentric Urban Structure: An Empirical Analysis Based on Multi-Source Big Data Fusion. *Remote Sens.* **2022**, *14*, 2705. [CrossRef]
32. Cao, X.; Shi, Y.; Zhou, L. Research on Urban Carrying Capacity Based on Multisource Data Fusion—A Case Study of Shanghai. *Remote Sens.* **2021**, *13*, 2695. [CrossRef]
33. Jun, Z.; Xiao-Die, Y.; Han, L. The Extraction of Urban Built-Up Areas by Integrating Night-Time Light and POI Data—A Case Study of Kunming, China. *IEEE Access* **2021**, *9*, 22417–22429. [CrossRef]
34. He, X.; Zhu, Y.; Chang, P.; Zhou, C. Using Tencent User Location Data to Modify Night-Time Light Data for Delineating Urban Agglomeration Boundaries. *Front. Environ. Sci.* **2022**, *10*, 860365. [CrossRef]
35. He, X.; Zhang, Z.; Yang, Z. Extraction of urban built-up area based on the fusion of night-time light data and point of interest data. *R. Soc. Open Sci.* **2021**, *8*, 210838. [CrossRef] [PubMed]
36. Zhang, J.; Yuan, X.; Tan, X.; Zhang, X. Delineation of the Urban-Rural Boundary through Data Fusion: Applications to Improve Urban and Rural Environments and Promote Intensive and Healthy Urban Development. *Int. J. Environ. Res. Public Health* **2021**, *18*, 7180. [CrossRef] [PubMed]
37. Zhou, C.; He, X.; Wu, R.; Zhang, G. Using Food Delivery Data to Identify Urban -Rural Areas: A Case Study of Guangzhou, China. *Front. Earth Sci.* **2022**, *10*, 860361. [CrossRef]
38. He, X.; Zhou, C.; Zhang, J.; Yuan, X. Using Wavelet Transforms to Fuse Nighttime Light Data and POI Big Data to Extract Urban Built-Up Areas. *Remote Sens.* **2020**, *12*, 3887. [CrossRef]
39. Wang, L.; Fan, H.; Wang, Y. Improving population mapping using Luojia 1-01 nighttime light image and location-based social media data. *Sci. Total Environ.* **2020**, *730*, 139148. [CrossRef]
40. Wang, J.; Hu, C.; Ma, B.; Mu, X. Rapid Urbanization Impact on the Hydrological Processes in Zhengzhou, China. *Water* **2020**, *12*, 1870. [CrossRef]
41. Li, X.; Zhu, J.; Yin, X.; Yao, C.; Huang, J.; Li, M. Mapping construction land of Guangzhou based on Luojia No. 1 nightlight data. *J. Geo-Inf. Sci.* **2019**, *21*, 1802–1810.
42. Shi, K.; Chen, Z.; Cui, Y.; Wu, J.; Yu, B. NPP-VIIRS Nighttime Light Data Have Different Correlated Relationships With Fossil Fuel Combustion Carbon Emissions From Different Sectors. *IEEE Geosci. Remote Sens. Lett.* **2020**, *18*, 2062–2066. [CrossRef]
43. Ortakavak, Z.; Çabuk, S.N.; Cetin, M.; Kurkcuoglu, M.A.S.; Cabuk, A. Determination of the nighttime light imagery for urban city population using DMSP-OLS methods in Istanbul. *Environ. Monit. Assess.* **2020**, *192*, 790. [CrossRef] [PubMed]
44. Shi, K.; Chang, Z.; Chen, Z.; Wu, J.; Yu, B. Identifying and evaluating poverty using multisource remote sensing and point of interest (POI) data: A case study of Chongqing, China. *J. Clean. Prod.* **2020**, *255*, 120245. [CrossRef]
45. Zikirya, B.; He, X.; Li, M.; Zhou, C. Urban Food Takeaway Vitality: A New Technique to Assess Urban Vitality. *Int. J. Environ. Res. Public Health* **2021**, *18*, 3578. [CrossRef] [PubMed]
46. Massout, S.; Smara, Y. Panchromatic and multispectral image fusion using the spatial frequency and the à trous wavelet transform. *J. Appl. Remote Sens.* **2021**, *15*, 036510. [CrossRef]
47. Gharbia, R.; Hassanien, A.E.; El-Baz, A.H.; Elhoseny, M.; Gunasekaran, M. Multi-spectral and panchromatic image fusion approach using stationary wavelet transform and swarm flower pollination optimization for remote sensing applications. *Future Gener. Comput. Syst.* **2018**, *88*, 501–511. [CrossRef]
48. Shu-Long, Z. Image fusion using wavelet transform. *Int. Arch. Photogramm. Remote Sens. Spat. Inf. Sci.* **2002**, *34*, 552–556.
49. Li, G.; Yang, H.; Wang, J.; Li, Y.; Zhang, C.; Xie, H.; Feng, B. PCA-based Wavelet Remote Sensing Image Synthesis Simulation Method. In Proceedings of the 2021 IEEE 5th Advanced Information Technology, Electronic and Automation Control Conference (IAEAC), Chongqin, China, 12–14 March 2021; Volume 5, pp. 1042–1046.
50. Cheng, J.; Liu, H.; Liu, T.; Wang, F.; Li, H. Remote sensing image fusion via wavelet transform and sparse representation. *ISPRS J. Photogramm. Remote Sens.* **2015**, *104*, 158–173. [CrossRef]
51. Hu, K.; Feng, X. Research on the multi-focus image fusion method based on the lifting stationary wavelet transform. *J. Inf. Process. Syst.* **2018**, *14*, 1293–1300.
52. Gao, J.; Wang, B.; Wang, Z.; Wang, Y.; Kong, F. A wavelet transform-based image segmentation method. *Optik* **2020**, *208*, 164123. [CrossRef]
53. Guobin, C.; Sun, Z.; Zhang, L. Road Identification Algorithm for Remote Sensing Images Based on Wavelet Transform and Recursive Operator. *IEEE Access* **2020**, *8*, 141824–141837. [CrossRef]

54. Drăguţ, L.; Csillik, O.; Eisank, C.; Tiede, D. Automated parameterisation for multi-scale image segmentation on multiple layers. *ISPRS J. Photogramm. Remote Sens.* **2014**, *88*, 119–127. [CrossRef] [PubMed]
55. Wang, Z.; Chen, G.; Yu, B.; Zhang, X. Determination of the optimal segmentation scale of high-resolution remote sensing images of islands and reefs in the south China sea. *Geosptial Inf.* **2018**, *16*, 21–24.
56. Zhao, G.; Dong, J.; Liu, J.; Zhai, J.; Cui, Y.; He, T.; Xiao, X. Different patterns in daytime and nighttime thermal effects of urbanization in Beijing-Tianjin-Hebei urban agglomeration. *Remote Sens.* **2017**, *9*, 121. [CrossRef]
57. Cui, Y.; Shi, K.; Jiang, L.; Qiu, L.; Wu, S. Identifying and Evaluating the Nighttime Economy in China Using Multisource Data. *IEEE Geosci. Remote Sens. Lett.* **2020**, *18*, 1906–1910. [CrossRef]
58. Liu, S.; Shi, K.; Wu, Y.; Chang, Z. Remotely sensed nighttime lights reveal China's urbanization process restricted by haze pollution. *Build. Environ.* **2021**, *206*, 108350. [CrossRef]
59. Yuan, H.; Wang, X.; Wu, C.; Wang, H. Satellite Observed Strong Relationship Between Nighttime Surface Temperature and Leaf Coloring Dates of Terrestrial Ecosystems in East China. *IEEE J. Sel. Top. Appl. Earth Obs. Remote Sens.* **2020**, *13*, 717–725. [CrossRef]
60. Wang, M.; Song, Y.; Wang, F.; Meng, Z. Boundary extraction of urban built-up area based on luminance value correction of NTL image. *IEEE J. Sel. Top. Appl. Earth Obs. Remote Sens.* **2021**, *14*, 7466–7477. [CrossRef]
61. Li, Q.; Zheng, B.; Tu, B.; Yang, Y.; Wang, Z.; Jiang, W.; Yao, K.; Yang, J. Refining urban built-up area via multi-source data fusion for the analysis of Dongting Lake eco-economic zone spatiotemporal expansion. *Remote Sens.* **2020**, *12*, 1797. [CrossRef]
62. Liu, L.; Leung, Y. A study of urban expansion of prefectural-level cities in South China using night-time light images. *Int. J. Remote Sens.* **2015**, *36*, 5557–5575. [CrossRef]
63. Li, L.; Zhou, H.; Wen, Q.; Chen, T.; Guan, F.; Ren, B.; Yu, H.; Wang, Z. Automatic extraction of urban built-up area based on object-oriented method and remote sensing data. *Int. Arch. Photogramm. Remote Sens. Spat. Inf. Sci.* **2018**, *42*, 877–883. [CrossRef]
64. He, X.; Zhou, C.; Wang, Y.; Yuan, X. Risk Assessment and Prediction of COVID-19 Based on Epidemiological Data From Spatiotemporal Geography. *Front. Environ. Sci.* **2021**, *9*, 634156. [CrossRef]
65. Wu, J.; Zhang, Z.; Yang, X.; Li, X. Analyzing Pixel-Level Relationships between Luojia 1-01 Nighttime Light and Urban Surface Features by Separating the Pixel Blooming Effect. *Remote Sens.* **2021**, *13*, 4838. [CrossRef]
66. Bu, L.; Xu, Z.; Zhang, G. Night-Light Image Restoration Method Based on Night Scattering Model for Luojia 1-01 Satellite. *Sensors* **2019**, *19*, 3761. [CrossRef]